Research Article | Vol. 30, No. 8 / 11 Apr 2022 / Optics Express 13009
Optics EXPRESS

Long seed, short pump: converting Yb-doped laser radiation to multi-µJ few-cycle pulses tunable through 2.5–15 µm

RIMANTAS BUDRIŪNAS,[1,2,*] KAROLIS JURKUS,[2] MIKAS VENGRIS,[1,2] AND ARŪNAS VARANAVIČIUS[1]

[1] Vilnius University Laser Research Centre, 10 Saulėtekio ave., LT-10223, Vilnius, Lithuania
[2] Light Conversion Ltd., 2b Keramikų st., LT-10233, Vilnius, Lithuania
[*] rimantas.budriunas@lightcon.com

Abstract: We present a setup for generating broadband (up to 1050 cm^{-1}) and broadly tunable (2.5-15 µm) mid-infrared pulses using an Yb-doped femtosecond laser as the pump source. Our scheme, comprising two parametric amplifiers and a mixing stage, exploits favorable group velocity matching conditions in GaSe pumped at 2 µm to directly produce sub-70 fs pulses throughout the tuning range without any additional dispersion compensation, while 30–50 fs pulse durations are achieved with simple dispersion compensation by propagation through thin bulk media. The generated pulses have sub-1% short- and long-term energy noise, as well as stable spectral parameters, while delivering 0.5–2 W average mid-IR power. We expect the source to be useful for various spectroscopic applications in the mid-IR.

1. Introduction

The fundamental vibrational resonances of many materials are located in the mid-infrared (mid-IR) spectral range 2–20 µm (500–5,000 cm^{-1}) [1–3]. This makes mid-IR short-pulsed sources essential tools for various structure-sensitive spectroscopic investigations of ultrafast processes in matter and interfaces between different materials. Spectroscopic techniques such as surface-selective sum frequency generation spectroscopy [4] or two dimensional and multi-dimensional vibrational spectroscopy [5] will especially benefit from high peak and average power broadband mid-IR sources allowing for coherent excitation and simultaneous probing of different vibrational-rotational states. Microjoule-level femtosecond mid-IR pulses are also essential for research in high harmonic generation from solids, allowing for all-optical investigations into band structure and electronic properties of materials [6–10]

A common way to produce broadband mid-IR pulses is nonlinear frequency down-conversion in difference frequency generation (DFG) or optical parametric amplification (OPA) set ups driven by Ti:sapphire laser systems [11–18]. Broadband pulse generation in Ti:sapphire laser-based OPA architectures typically relies on short pump pulse duration to produce pulses with intrinsically short durations and therefore large bandwidth. This approach has the important advantage of producing short pulses directly at the exit face of the crystal, eliminating the need for additional pulse compressors, which may be complicated to build if expected to operate through a wide tuning range. In this approach, there is often a direct trade-off between the thickness of the DFG crystal and mid-IR bandwidth. Numerous more complex setups involving specialized manipulations on the interacting beams or alternative interaction geometries have been proposed [19–21].

The development of lasers operating at ~2 µm opened possibilities for improving mid-IR pulse generation efficiency using parametric amplifiers based on non-oxide crystals such as $ZnGeP_2$ (ZGP). Generation of broadband mid-IR pulses with energies up to several hundreds of microjoules was demonstrated in chirped pulse optical parametric amplification (OPCPA)

#455180 https://doi.org/10.1364/OE.455180
Journal © 2022 Received 10 Feb 2022; revised 16 Mar 2022; accepted 17 Mar 2022; published 4 Apr 2022

Optics EXPRESS

systems pumped by lasers with Ho-doped gain medium and operating at fixed mid-IR wavelengths [22–24]. Recently, generation of pulses tunable in the 2–8 μm range with average power of few tens of mW and bandwidth corresponding to few cycle pulses has been demonstrated using ZGP OPA pumped by 3 ps pulses from Ho:YLF regenerative amplifier [25] while another system reached multi-W average power and multi-mJ pulse energy at 5 μm [26]. However, in these works pump pulse durations were in range of 1–16 ps, and in all cases additional compressors at the output of the systems had to be used in order to produce pulses shorter than 200 fs. Broadband ~ 1 μJ pulses with average power in excess of 150 mW tunable in 4–18 μm were generated using intrapulse DFG in GaSe when pumped by 16 fs nonlinearly compressed pulses from Tm-doped fiber laser [27]. A similar intrapulse DFG scheme was also demonstrated with a Ho:YAG thin disk oscillator followed by nonlinear compression stage [28]. Efficient (>3%) mid-IR transient generation at comparable average power (150 mW) was also demonstrated using a 2.5 μm, 20 fs Cr:ZnS laser system as the pump source [29].

Another option for femtosecond mid-IR pulse generation is the class of already highly mature laser technologies emitting at ~1 μm wavelength, including laser materials doped with Nd- and Yb- ions. Compared to 800 nm and 2 μm pump platforms it offers a substantially broader selection of ultrashort-pulsed lasers with distinguished achievements in energy and power scaling, featuring versatile repetition rates and unmatched energy stability. However, despite these advantages, limitations for broadband mid-IR sources typically arise due to the inherently longer durations of Yb-doped laser pulses as compared to that of Ti:sapphire. When basic OPA architectures similar to those traditionally employed with Ti:sapphire lasers are used with Yb-based lasers, the longer laser pulse duration typically results in output pulses with correspondingly longer pulse durations and narrower bandwidths on the level of 100 cm^{-1} [5,30,31]. This may make such systems unattractive for spectroscopic applications requiring broadband pulses.

Conversely, the longer pulse duration of Yb- and Nd-doped lasers can also be a favorable property when the more complex OPCPA concept is applied. Such solutions have shown some excellent results in producing mid-IR pulses as short as a few optical cycles [32–38] with energies up to 35 mJ at 3.9 μm at 20 Hz [32], while several systems operating at ≥100 kHz repetition rates demonstrated average powers well exceeding 10 W at ~3 μm [33,39,40]. However, in many cases, such setups rely on a particular phase matching condition, resulting in broadband amplification around a nearly fixed output wavelength, and rapidly decreasing pulse bandwidth and/or conversion efficiency as the output wavelength is shifted away from the favorable wavelength [41,42]. Furthermore, the OPCPA concept, by definition, involves compressing the amplified pulses, and designing pulse compressors that operate through a broad mid-IR tuning range is challenging. Meanwhile, mid-IR spectroscopic applications often benefit from light sources that are tunable across the molecular fingerprint spectral range without significant changes in source configuration and performance characteristics. Several architectures providing generation of wavelength tunable broadband pulses via DFG between Yb laser driven tunable OPA and laser fundamental [35,43,44], mixing signal and idler from an OPA [5] or near–IR signal down-conversion in LGS based OPA [4,31,44] were demonstrated.

In this study, we report an alternative scheme for generation of multi-microjoule energy pulses with bandwidth corresponding to a few optical cycles tunable in 2.5–15 μm range (pulse central wavelengths). Mid-IR pulses are produced by mixing the outputs of two-channel parametric amplification setup, consisting of one channel producing 30 fs pulses at a fixed wavelength around 2 μm, and another channel producing narrowband seed pulses tunable through 2.2–4 μm. This wavelength combination allows us to leverage the favorable dispersion and nonlinear properties of gallium selenide (GaSe) crystal to produce mid-infrared DFG output with spectral components from <4 μm to >17 μm, while wavelength components from <2.5 μm to >5 μm are accessible by taking the amplified seed pulses, which are shortened due to the temporal gating by the short pump pulse. Finally, we demonstrate that, at the expense of some pulse energy, the

Optics EXPRESS

setup can produce very broadband pulses around 9 μm, with significant spectral intensity from 6 μm to 15 μm (>700 cm^{-1} FWHM bandwidth). This makes the proposed scheme an attractive choice for applications that require multi-μJ broadband mid-infrared pulses, such as vibrational sum-frequency generation spectroscopy.

2. Experimental setup

A block diagram of the experimental setup is shown in Fig. 1(a). Pump laser light is split in a 9:1 ratio to pump two parametric amplifier chains. The larger part of pulse energy is used to pump a fixed-wavelength, broadband NOPA producing pulses around 2 μm. The remaining part of energy is sent to a tunable narrowband OPA (more details on the two OPAs will be given later in the text). Finally, the outputs of the two OPA channels are combined on a dichroic mirror at a small intersection angle and mixed in a gallium selenide (GaSe) crystal to produce two tunable mid-IR outputs: a difference frequency pulse and the amplified seed pulse, which is substantially shortened due to temporal gating by the short pump pulse. In case of low group velocity mismatch and dispersive pulse broadening in the amplification crystal, this approach can be expected to yield short pulses irrespective of seed wavelength, as the pulse duration is firmly set by the short pump pulse, which is not tuned. The situation is depicted schematically in Fig. 1(b).

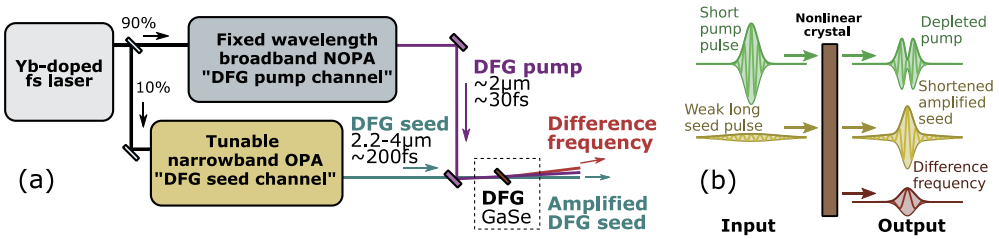

Fig. 1. (a) Block diagram of the experimental setup (b) Illustration of the pulses interacting in the difference frequency generation (DFG) stage

Figure 2 shows group velocity mismatch curves between signal and idler (solid lines) and pump and idler (dashed lines) for output (idler) wavelengths in the 4–17 μm range in several popular crystal and pump wavelength combinations. Group velocity mismatch data for our chosen configuration of a fixed 2 μm pump wavelength and GaSe crystal is plotted in blue. Orange and green lines show two typical situations occurring in Ti:sapphire-based systems using $AgGaS_2$ (AGS) and GaSe crystals, respectively. Red lines show group velocity mismatch in one of the relatively few configurations allowing direct pumping at 1030 nm using $LiGaS_2$ (LGS) crystal. As seen from the curves, the lowest group velocity mismatch, and hence the broadest possible amplification bandwidth and lowest pulse broadening is provided by AGS crystals pumped at 1.4 μm (akin to the situation encountered in Ti:sapphire-based systems) [17]. Unfortunately, AGS crystals are not suitable for high repetition rate systems, as they degrade quickly upon exposure to intense femtosecond pulse radiation (typically lasting several thousand hours at 1 kHz repetition rate, and correspondingly degrading within hours or faster in a 100 kHz system in our own trials) [45]. For the same pump wavelength, GaSe provides slightly worse group velocity matching, but ensures longevity, as GaSe crystals do not exhibit obvious long-term degradation. LGS has the significant advantage of the possibility for direct pumping at 1030 nm and has been demonstrated to be capable of near-single-cycle pulses around 7–8 μm [44], but achievable pulse durations away from this wavelength are strongly limited by rapidly degrading phase- and group velocity-matching conditions, while crystal transparency range limits output wavelength components to below ~12 μm [46]. Our chosen configuration of GaSe pumped at 2

Optics EXPRESS

μm provides a good compromise of broad crystal transparency (up to >16 μm [47]), longevity, and a relatively low group velocity mismatch between the interacting waves over most of the range, as well as far higher nonlinearity than the other considered crystals.

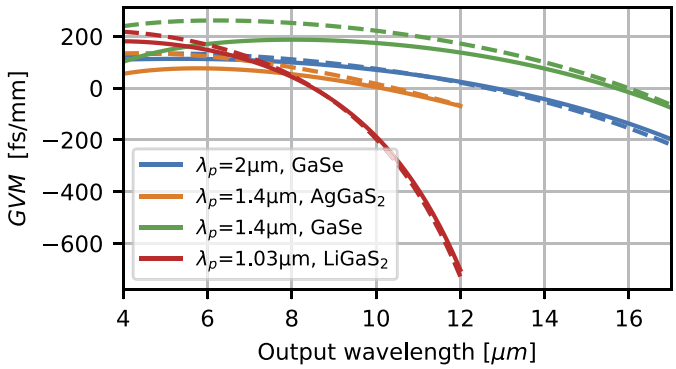

Fig. 2. Variation of group velocity mismatch (GVM) with change of idler wavelength in several popular combinations of crystals and pump wavelengths λ_p. *Solid lines*: GVM between signal and idler; *dashed lines:* GVM between pump and idler. GaSe pumped at 2μm exhibits a moderate GVM over a broad wavelength range, with full group velocity matching (identical group velocities for pump, signal and idler waves) occurring around 13μm.

Three pump laser (Pharos-PH2 and Carbide-CB3, Light Conversion) configurations were tested for pumping the OPA setup to investigate the capability to adjust our design for applications prioritizing either higher pulse energy or higher pulse repetition rate. Maximum average laser power used was 80 W, while the highest tested pump pulse energy was 2 mJ. Pump laser parameters are summarized in Table 1. In all cases, pump pulse duration was ~200 fs. Re-configuration of the OPA setup between different laser configurations involved changing of lens telescopes and ratios of internal beam splitters to maintain similar pump intensity on all amplification stages at the different pump energies. However, the general architecture of the system remained unchanged.

Table 1. Pump laser configurations used in the experiments

#	Pump laser	Pulse repetition rate	Average pump power	Pump pulse energy
1	Pharos-PH2	10 kHz	20 W	2 mJ
2	Carbide-CB3	400 kHz	80 W	200 μJ
3	Carbide-CB3	50 kHz	80 W	1.6 mJ

Because of the noncollinear geometry employed in the DFG stage to facilitate separation of the pump, signal and idler beams, the difference frequency is angularly dispersed [48]. Generally, this is not ideal, as this leads to a DFG pulse with a tilted pulse front, which lengthens the effective pulse duration and lowers the peak intensity [49]. However, the noncollinear geometry avoids losses and additional dispersion that could be introduced by the filtering optics, and mid-infrared pulses produced in noncollinear DFG geometry have been successfully used in numerous works [8,16,50–54]. Ultimately, although we had to rely on the noncollinear geometry to separate the interacting waves due to lack adequate optics at the time of the experiments, suitable optical elements are available and their use was demonstrated by other groups in comparable conditions [28,55], while reconfiguring the setup to collinear operation for simplified alignment and angular dispersion-free DFG beam would be trivial.

Optics EXPRESS

3. Parameters of the dual parametric amplifiers and mixing stage

The broadband NOPA channel, the output of which is used as the pump pulse in the DFG stage, exploits broadband phase matching available in Type-I OPA crystals near degeneracy, which allows for broadband amplification around 2 μm when using ~1 μm pump lasers. Initial seed pulses for the broadband NOPA channel are derived from white light generated in a YAG crystal pumped at the laser fundamental wavelength. Loose focusing of the white light pump beam is used to achieve the required octave-spanning red-shifted spectral broadening [56,57]. The white light seed is amplified in three amplification stages based on BBO crystals cut for Type-I phase matching. In all three pump laser configurations, 2 mm thick BBO crystals are used in all three NOPA stages, pumped at intensities in the range of 200–250 GW/cm^2. A typical NOPA output spectrum and autocorrelation of the output pulse from the DFG pump channel after compression are given in Fig. 3(a) and Fig. 3(b), respectively. The white light seed spectrum is also shown in Fig. 3(a) for comparison. Total pump-to-signal conversion efficiency is 11–12% in this channel, resulting in 200 μJ pulses (2 W average power) in Configuration 1, 20 μJ (8 W average power) in Configuration 2, and ~160 μJ in Configuration 3.

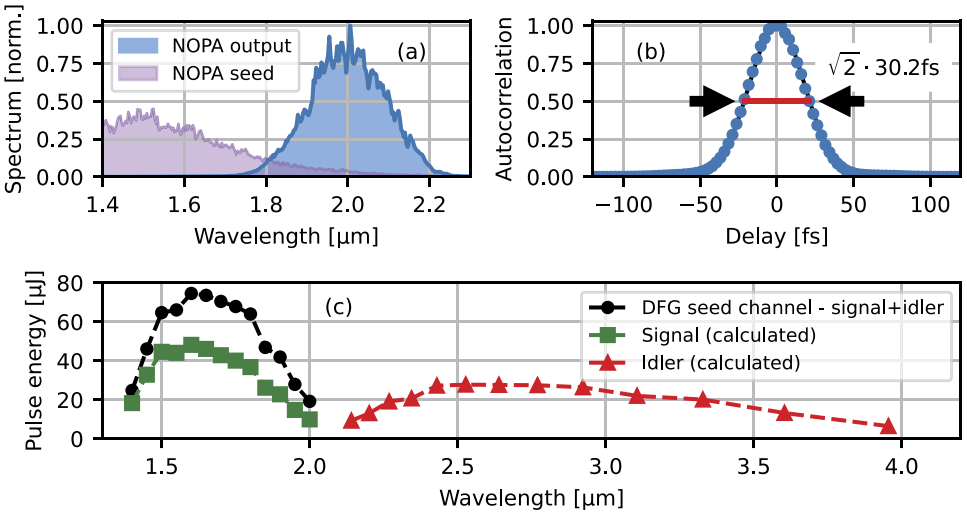

Fig. 3. Typical parameters of the two OPA channels. (a) Spectrum of the DFG pump NOPA channel output and the relevant portion of its white light seed spectrum (intensity of the white light spectrum is not to scale) (b) autocorrelation trace of the DFG pump OPA pulse. Blue dots: measured data points; black line: Gaussian fit. The pulse duration is 30.2 fs (c) Pulse energies of the DFG seed channel OPA at different output wavelengths, measured in Configuration #1.

The DFG seed channel is a typical two-stage, band-limited OPA operated in a collinear geometry. The seed pulse is again derived from a white light continuum generated in a YAG crystal. The continuum pulse is temporally stretched in a silicon window to produce nearly transform-limited pulses with nearly Gaussian spectra of 100–150 cm^{-1} FWHM bandwidth. Both stages use 5 mm thick KTA crystals pumped at the laser fundamental wavelength at intensities of 50–75 GW/cm^2. After separating the signal and idler beams by a dichroic mirror that reflects the signal, the idler of the second stage of this OPA channel, tunable from 2.2 μm to 4 μm, is used as the DFG seed beam in the mixing stage. Pulse energies in the DFG seed channel, achieved at different wavelengths, measured in Configuration 1, are shown in Fig. 3(c). Similar conversion efficiencies are achieved in the other configurations.

Optics EXPRESS

In order to generate pulses with central wavelengths above 11-12 μm and up to 15 μm, the bandwidth of 2 μm pump pulses had to be reduced. This is achieved simply by inserting an additional 5 mm thick silicon window into the seed white light in the NOPA channel to increase the chirp of the white light seed. 2 μm pulse bandwidth is reduced to ~150 cm^{-1} and output pulse duration is measured to be 140 fs with nearly Gaussian temporal and spectral profiles, while very similar pulse energy is maintained.

After being combined on a dichroic mirror, the pulses from the two OPA channels are mixed in a 0.75 mm GaSe crystal. Crossing angle is kept as low as possible whilst still allowing for separation of the beams (below 0.5°). In Configuration 1, the measured $1/e^2$ diameter of the 2 μm pump beam on the GaSe crystal was 2 mm, corresponding to on-crystal peak intensity of 400 GW/cm^2 in the broadband configuration (not accounting for reflection losses). As beam diameters are not changed for narrowband operation, the intensity drops to about 85 GW/cm^2 when switching to narrowband mode due to the longer 2 μm pulse duration. Diameter of the seed beam varied with wavelength from 1.5 mm to 2.2 mm ($1/e^2$ level), while estimated intensity varied between 1 and 10 GW/cm^2. In other configurations, beam diameters were reduced to maintain approximately the same pump intensities.

4. Mid-infrared generation results

4.1. Mid-IR spectra

As the key goal of this work was to create a broadband mid-IR source, we first discuss the spectral properties of the generated mid-IR radiation. Due to the broad output wavelength range, several devices had to be used to characterize the spectra. Most measurements were performed using a scanning FTIR spectrometer (FTIR, Light Conversion). In several cases, we also used a scanning monochromator (Kymera, Andor) to obtain higher resolution spectra. Both devices were equipped with an MCT detector (PDAVJ10, Thorlabs). The dropping sensitivity of this detector above 10 μm and, in case of the monochromator, overlapping diffraction orders made measurements above 10 μm difficult. Therefore, for longer wavelengths, we also used a home-built imaging spectrometer based on a ZnSe prism as the dispersive element and a microbolometer array camera (WinCamD-IR-BB, DataRay) as the detector. With this device, we were able to measure spectral components up to >17 μm. The resolution of the home-built spectrometer was estimated to vary between ~100 cm^{-1} at 6 μm and ~65 cm^{-1} at 8 μm to better than 20–40 cm^{-1} in the 10–15 μm range.

Typical spectra of the mid-IR outputs achieved with the three pump laser configurations are shown in Fig. 4(a-c). Pulses with central frequencies higher than ~2300 cm^{-1} are produced in the amplified DFG seed beam, while pulses at lower central frequencies are obtained from the DFG beam. Overall, bandwidths over 200 cm^{-1} are maintained throughout the range in all broadband configurations, while significantly broader bandwidths up to 1050 cm^{-1} are achieved in some spectral regions, including the important OH and OD vibration ranges. It is notable that the pulses in the seeded beam retain a narrow spectral feature at the seed wavelength, but the spectra are broadened substantially due to temporal gating by the short pump pulse. In the reduced bandwidth configuration used to access 12–15 μm central wavelengths, output bandwidth is around 150–170 cm^{-1}.

If the DFG stage is set to favor phase matching at the edges of the DFG spectrum, still broader bandwidths at longer wavelengths can be achieved, at the expense of some pulse energy (up to two-fold efficiency loss compared to an optimized-for-energy configuration). Some examples of spectra obtained when the DFG stage is optimized for broader bandwidth are shown in Fig. 5(a). Bandwidths exceeding 700 cm^{-1} (FWHM) are possible around 9 μm.

The calibration of the prism spectrometer was verified by comparing the signals obtained with and without a silicon window because silicon has easily identifiable absorption features in the 7–18 μm range. The results are shown in Fig. 5(b). Measured spectra were corrected for

Optics EXPRESS

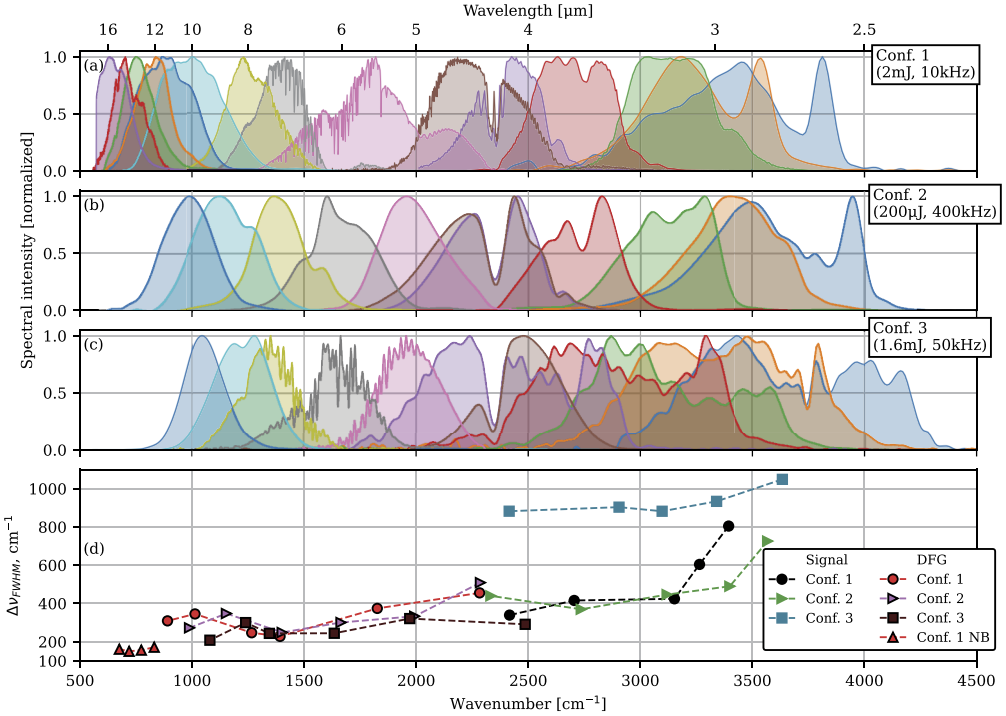

Fig. 4. (a-c) Typical spectra recorded in three configurations throughout the tuning range, showing continuous coverage with spectral components from >16 μm to <2.5 μm. (d) FWHM bandwidths calculated for the spectra. Signal and idler ranges are shown as separate lines for each configuration. The narrowband mode, allowing generation of pulses with central wavelengths >12 μm, is listed separately. Atmospheric absorption features (water vapor around 2.7 μm and 6 μm and CO_2 at 4.2 μm) are visible on the spectra.

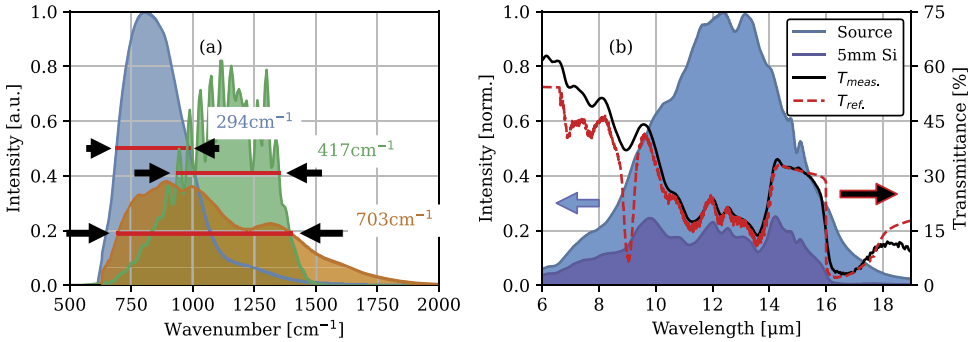

Fig. 5. (a) Examples of spectra measured at longer wavelengths when system was tuned for broader bandwidth (10 kHz configuration) (b) Example of prism spectrometer calibration. Blue shaded area: measured spectrum; Purple shaded area: spectrum measured with a 5 mm-thick silicon window inserted before the spectrometer; black line: transmittance of silicon estimated from the ratio of the two measured spectra; dotted red line: reference transmission data provided by the supplier of the silicon window (Thorlabs)

Optics EXPRESS

the slight variation of detection sensitivity in the 6–18 μm range. It is seen that key absorption features are clearly represented from 7 μm to 17 μm within a single spectrum, confirming the spectral extent of the pulses.

It should also be noted that, as the signal and DFG outputs are a signal-idler pair, they are not independently tunable, but available simultaneously and well-synchronized. Therefore, in some cases, such as experiments requiring multi-pulse, multi-wavelength excitation, both outputs may be useful at the same time, utilizing the output power more efficiently.

4.2. Mid-IR pulse durations

Durations of amplified seed and DFG pulses were measured using the SFG-XFROG technique [58]. A small part of the energy of the pump laser pulse at ~1 μm was split off from the pump beam of the final OPA stage of the DFG pump OPA channel, and delay-matched to the output pulses. The transform-limited 190 fs duration of these pulses provided a good compromise between spectral and temporal resolution for the XFROG measurements. Very thin nonlinear crystals, chosen appropriately for the wavelength ranges, were used for SFG to ensure distortion-free measurements (10 μm thick BBO [59] for signal range, 35 μm thick GaSe for DFG range). The measurements were performed in Configuration 3.

Pulse measurements at four wavelengths are presented in detail in Fig. 6. A measurement of a signal-range pulse is shown in Fig. 6(a-d). A 3 mm CaF_2 window had to be used to compress the pulse to nearly transform-limited 31.6 fs duration. The slight tail of the pulse seen in the retrieved time-domain profile (Fig. 6(c)) originates from the longer seed pulse. Figure 6(e-h) show a measurement of a pulse around 4.5 μm, in which the spectral dip and temporal post-pulse due to the CO_2 absorption are clearly visible [60]. An example of a DFG pulse at 8.9 μm is given in Fig. 6(i-l). As the dispersion of GaSe is strongly negative at 8.9 μm, we used a 1 mm-thick germanium plate to compress the pulse and achieve sub-1.5-cycle pulse duration. In this case, the post-pulse is due to relatively large uncompensated third-order dispersion. Finally, Fig. 6(m-p) shows a measurement at 10.9 μm, the longest wavelength at which XFROG measurements were performed.

Pulse durations measured throughout the tuning range are summarized in Fig. 7. Pulse durations without any additional dispersion compensation and with simple windows used for compression are shown.

It is seen that sub-70 fs durations are maintained throughout the tuning range directly from the DFG crystal. In general, the produced pulses are no more than 1.5–1.7 times longer than their respective transform limits, which confirms the expectation that pulse broadening in the GaSe crystal should be low. It was noted that some positive chirp was not compensated by the 3 mm CaF_2 window at 2.7 and 3 μm, while measured chirp turned notably negative at 3.8 μm. Hence, it can be expected that using a CaF_2 windows with different thicknesses, ~30 fs pulses may be achieved in most of the signal range. On the other hand, pulse duration at 9–10 μm is limited by the large third order dispersion of optical materials in that range, and it appears unlikely that compressed pulse durations could be improved much by changing the thickness of the germanium window.

4.3. Achieved power and conversion efficiency

Pulse energies and powers obtained at wavelengths throughout the tuning range in different pump laser configurations are shown in Fig. 8. Note that an additional narrowband operation mode (described in Section 3) had to be used to tune the central wavelength of output pulses above 11–12 μm. Preliminary investigations show that this tuning limitation stems from the combination of parametric gain asymmetry (favoring higher frequencies of the DFG pulse) and broadband phase matching in GaSe around 11–15 μm. We emphasize that the tuning limitation concerns only the tuning of *central frequency* of the output pulses; as shown in Fig. 5, spectral

Optics EXPRESS

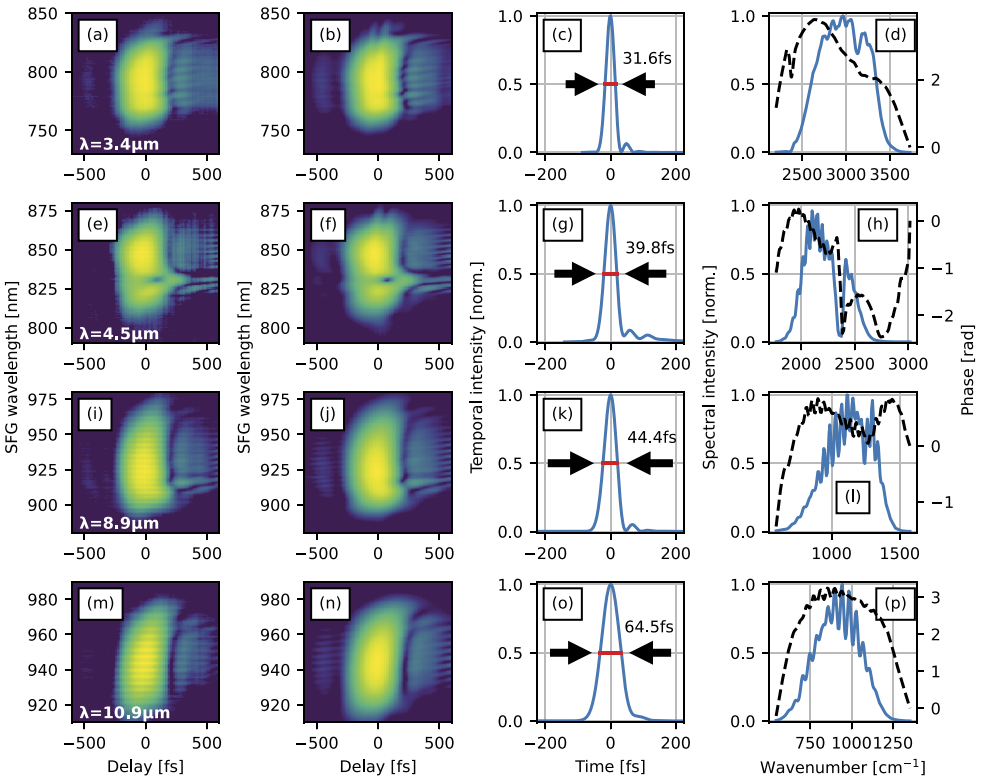

Fig. 6. SFG-XFROG measurements of generated mid-IR pulses. Columns 1 and 2: measured and retrieved XFROG traces, respectively; Column 3: retrieved pulse profiles; Column 4: retrieved spectra and spectral phases. Each row represents measurement at a different wavelength (3.4 μm, 4.5 μm and 8.9 μm, 10.9 μm). The fast modulations seen in the retrieved spectra are due to a reflection in the thin measurement crystal.

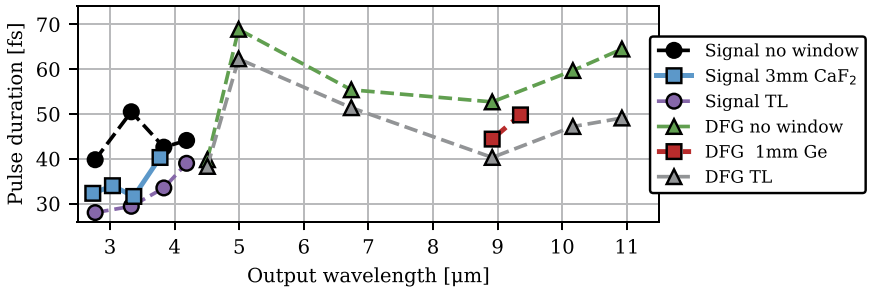

Fig. 7. Pulse duration measured throughout the tuning range of the device (50 kHz configuration). Pulse durations are measured without any additional dispersion control means, and, for some wavelength ranges, with appropriately selected CaF_2 or Ge windows inserted. Transform-limited (TL) pulse durations are also indicated.

Optics EXPRESS

components well above 15 µm are readily generated in broadband mode as well. More details on these limitations concerning generation of broadband pulses in GaSe at >10 µm central wavelengths will be discussed in a separate study. Narrowband operation was only tested with laser configuration 1.

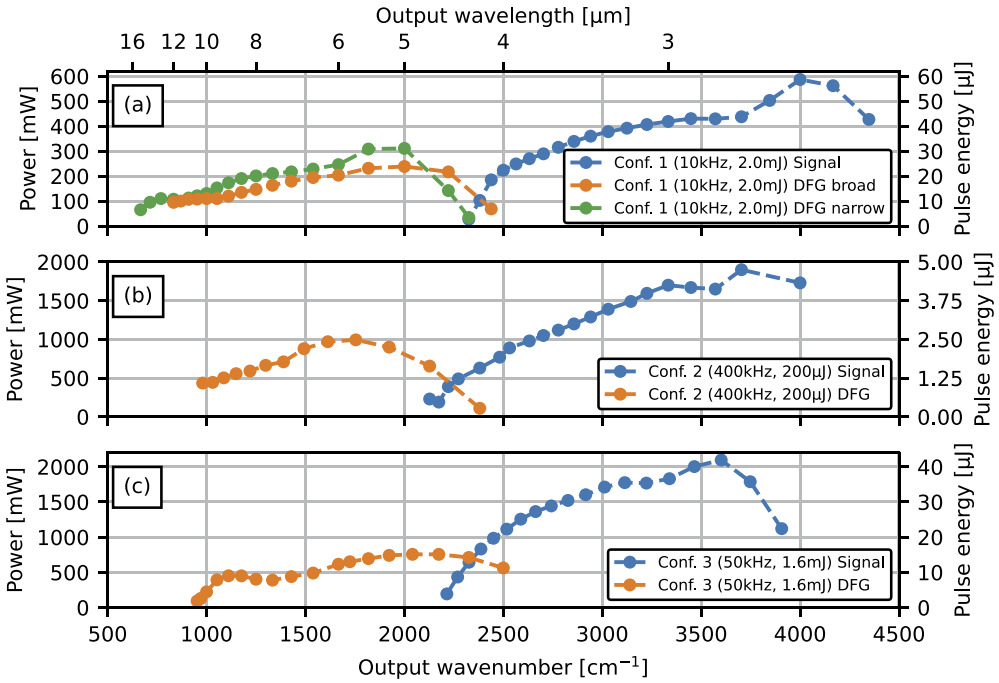

Fig. 8. (a-c) Output powers at different wavelengths throughout the tuning range in the three pump laser configurations. Narrowband operation, which allows for tuning to longer output wavelengths was only tested in configuration 1.

On average through the three configurations, total energy conversion efficiency from pump laser light to mid-IR output is around 2% at 3 µm, 1% at 6 µm, and 0.6% at 9 µm. While substantially higher conversion efficiency into ~3 µm pulses (7.6%) was demonstrated in [40], where a 3 µm pulse is amplified directly using the 1030 nm output from an Yb-doped laser as the pump, the authors noted that performance degraded rapidly when the system was tuned away from the design wavelength; furthermore, our setup provides slightly shorter pulses (31.6 fs compared to 38.2 fs in [40]) without active spectral phase control. Interestingly, the efficiency of our setup at 9 µm is slightly higher than that demonstrated in [35], despite our use of a cascaded OPA + DFG scheme as opposed to the direct OPA scheme in [35] (9 µm output generated as idler of OPA pumped by laser fundamental with no intermediate wavelength conversion step). Although more recent developments of LGS and BGS-based OPAs have shown substantially higher efficiencies exceeding 3% [61], average power scaling at wavelengths >8 µm with LGS crystals may eventually be limited by thermal effects due to the absorption gradually increasing from 8 µm up to the ~12 µm infrared cutoff [46,62], while GaSe exhibits substantially superior transparency up to 16 µm.

In configurations using the 80 W pump laser, output powers above 450 mW are maintained up to 9–10 µm (e.g. 503 mW at 9.2 µm in Conf. 2), which is, to the best of the authors' knowledge, the highest average output power reported in the literature for µJ-level femtosecond laser systems in the 9-10 µm wavelength range so far, including systems directly pumped by 2 µm and 3 µm

Optics EXPRESS

lasers and LGS-based schemes [15,16,27,35,61]. While in our experiments the average power was limited by pump laser power, evidence in the literature suggests that thermal effects in the BBO crystals used in the DFG pump NOPA channel could become limiting factors with only a modest pump laser power increase [63]. However, it has been shown that other crystals can be used instead of BBO to produce 2 µm OPA output of comparable parameters at substantially higher average powers [63–65], thus allowing further power scaling of the DFG pump channel, provided higher pump laser power is available. Some additional power scaling limitations can also be expected from atmospheric absorption of the DFG pump beam [66], however, this could be solved by purging the OPA enclosures to eliminate water vapor. On the other hand, GaSe crystals have been shown to be capable of handling much higher average pump powers at 2 µm than our current maximum of 8 W [27], thus the DFG stage should allow substantial power scaling.

4.4. Average power stability, shot-to-shot pulse energy stability and spectral stability

As these sources of infrared pulses are often used in experiments where data collection takes extended periods of time, it is vital that the parameters of the source remain as constant as possible over the measurement time. Although our dual-OPA setup is a step up in complexity, compared to typical Ti:sapphire-based DFG schemes, we demonstrate that, due to the compact and robust mechanical design of the OPA enclosure (total footprint 1.2×0.4 m^2, excluding the space for wavelength separation after the DFG crystal) and the consistent operation of the industrial-grade pump laser, this complexity does not result in stability penalties. Figure 9(a) shows average power measurements over 12 hours in signal and DFG wavelength ranges performed for the different configurations. Shot-to-shot pulse energy stability was also characterized by sampling the response of an MCT photodiode, logging every pulse over 24 seconds in the 50 kHz configuration.

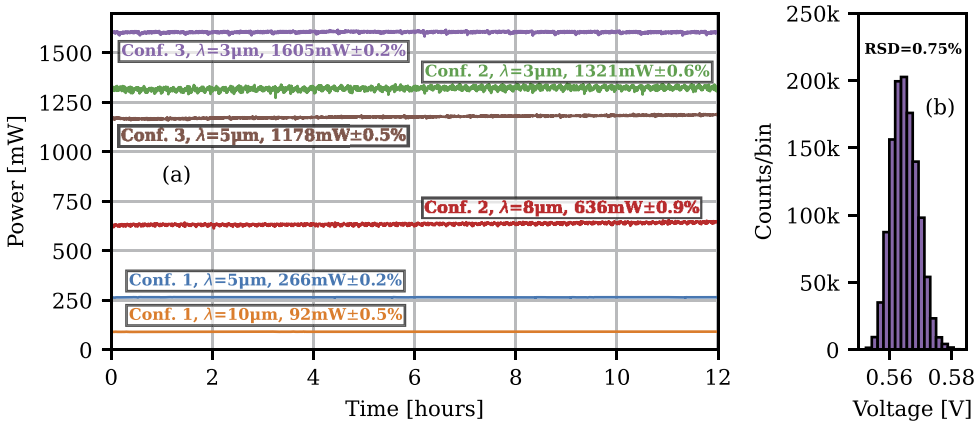

Fig. 9. Output stability parameters. (a) Long-term stability of average output power in the different configurations. Wavelengths, average powers and standard deviations are indicated in the text boxes (b) Shot-to-shot pulse energy stability measurement at 5 µm, measured in configuration 3 over 24 seconds (1.2M laser shots). The relative standard deviation (RSD) of pulse energies is 0.75%.

As the mid-IR output in our setup is produced by nonlinear interaction between two separate OPA channels, it is not a given that the temporal drift between the two OPAs would not result in a drift of output wavelength. We aim to minimize the sensitivity to temporal drift by using narrowband seed pulses that are longer than the pump pulses, but no specific dispersion control

Optics EXPRESS

methods are employed in the narrowband channel besides the initial seed pulse stretching. Because of this, the seed channel pulses are not strictly transform-limited, and a temporal delay drift may introduce a drift of output wavelength. To investigate if this was the case, we recorded output spectra of the system in the 10 kHz configuration with the prism spectrometer for an hour. The recorded spectra and their statistics are shown in Fig. 10. It should be noted that, as the camera used in the spectrometer has a time constant of 14 ms, the measurements are inherently averaged over multiple thousands of pulses, and hence information on possible shot-to-shot jitter is not obtained.

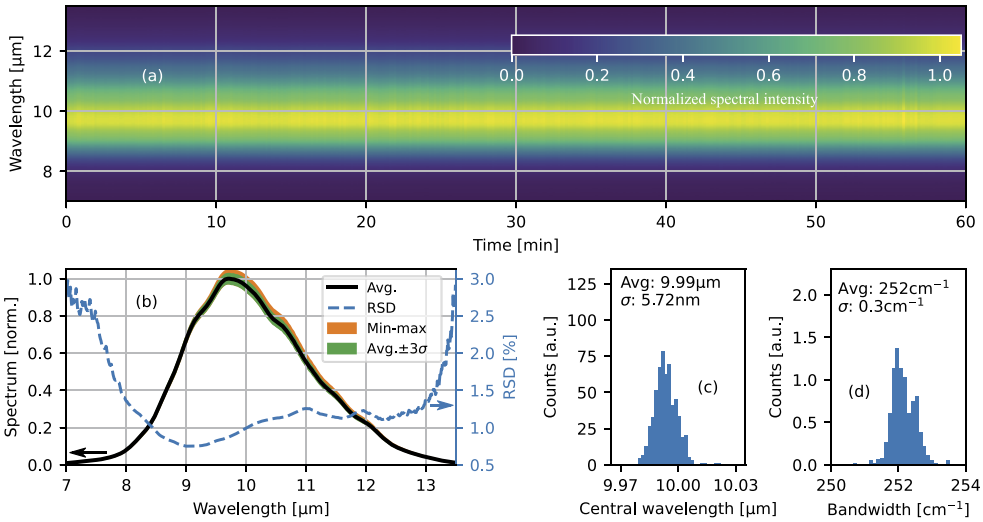

Fig. 10. Spectral stability at 10µm. (a) Spectra recorded over the 1-hour measurement. Note that the spectra are normalized to the average of peak intensities of all spectra, rather than the maximum of the full dataset. (b) Average spectrum and statistical boundaries of its variation (c,d) histograms of central wavelength and FWHM bandwidth, respectively, calculated for each recorded spectrum

As seen from the measurements, the output spectrum does not show discernable drift, with central wavelength and bandwidth varying well below the level of spectrometer resolution over the measurement period, and intensity at each wavelength component within $1/e^2$ bandwidth does not vary more than 1.5% over the hour. Therefore, we conclude that the two-channel OPA architecture does not cause spectral stability issues.

5. Conclusions and outlook

We have demonstrated a setup for generating broadband and broadly tunable (2.5–15 µm) mid-IR pulses starting from an Yb-doped amplified laser system, based on mixing the outputs of two optical parametric amplifiers (broadband 2 µm and tunable 2.2–4 µm) in a GaSe crystal. The carefully selected combination of OPA wavelengths and DFG crystal allows us to generate pulses with sub-70 fs durations and 200–1050 cm^{-1} bandwidths in a tuning range of 2.5–11 µm. With minimal dispersion adjustments, pulse durations as short as sub-3-cycle (31.6 fs) at 3.4 µm and 1.5-cycle (<45 fs) around 9 µm are achieved. Central wavelengths up to 15 µm are accessible with slightly narrower bandwidths (~150 cm^{-1}) with only a minor system reconfiguration. Despite the relatively complex two-channel architecture, we have demonstrated that the system maintains sub-1% power stability for multiple hours and maintains stable spectral parameters.

Optics EXPRESS

The setup was tested with 20 W and 80 W pump laser power and 200 µJ – 2 mJ pump pulse energy. We generated up to 450 mW power at 10 µm and 2 W at 2.5 µm with multi-µJ level pulse energy. In principle, the setup can be adapted for use with various fs to few-ps Yb-based laser platforms and scaled to different pulse energy or repetition rate regimes within the scope of parameters achieved by current femtosecond Yb-based lasers to fit the requirements of specific applications.

We expect that the short pulse durations available through a very broad tuning range, high average power and broad spectral coverage will make the setup an attractive source for various applications in time-resolved infrared spectroscopy.

Funding. European Regional Development Fund (01.2.2-LMT-K-718-01-0014).

Acknowledgments. The authors thank Karolis Neimontas and Darius Gadonas for valuable discussions throughout the experimental campaigns and Jonas Berzinš for suggestions on improving the manuscript.

Disclosures. RB, KJ, MV: Light Conversion (E)

Data availability. Data underlying the results presented in this paper may be obtained from the authors upon reasonable request.

References

1. A. Schliesser, N. Picqué, and T. W. Hänsch, "Mid-infrared frequency combs," Nat. Photonics **6**(7), 440–449 (2012).
2. H. Pires, M. Baudisch, D. Sanchez, M. Hemmer, and J. Biegert, "Ultrashort pulse generation in the mid-IR," Prog. Quantum Electron. **43**, 1–30 (2015).
3. J. Haas and B. Mizaikoff, "Advances in Mid-Infrared Spectroscopy for Chemical Analysis," Annu. Rev. Anal. Chem. **9**(1), 45–68 (2016).
4. Z. Heiner, L. Wang, V. Petrov, and M. Mero, "Broadband vibrational sum-frequency generation spectrometer at 100 kHz in the 950-1750cm −1 spectral range utilizing a $LiGaS_2$ optical parametric amplifier," Opt. Express **27**(11), 15289–15297 (2019).
5. P. M. Donaldson, G. M. Greetham, D. J. Shaw, A. W. Parker, and M. Towrie, "A 100 kHz Pulse Shaping 2D-IR Spectrometer Based on Dual Yb:KGW Amplifiers," J. Phys. Chem. A **122**(3), 780–787 (2018).
6. S. Ghimire, A. D. DiChiara, E. Sistrunk, P. Agostini, L. F. DiMauro, and D. A. Reis, "Observation of high-order harmonic generation in a bulk crystal," Nat. Phys. **7**(2), 138–141 (2011).
7. H. Liu, Y. Li, Y. S. You, S. Ghimire, T. F. Heinz, and D. A. Reis, "High-harmonic generation from an atomically thin semiconductor," Nat. Phys. **13**(3), 262–265 (2017).
8. M. Hohenleutner, F. Langer, O. Schubert, M. Knorr, U. Huttner, S. W. Koch, M. Kira, and R. Huber, "Real-time observation of interfering crystal electrons in high-harmonic generation," Nature **523**(7562), 572–575 (2015).
9. G. Vampa, T. J. Hammond, N. Thiré, B. E. Schmidt, F. Légaré, C. R. McDonald, T. Brabec, D. D. Klug, and P. B. Corkum, "All-Optical Reconstruction of Crystal Band Structure," Phys. Rev. Lett. **115**(19), 193603 (2015).
10. G. Vampa, T. J. Hammond, M. Taucer, X. Ding, X. Ropagnol, T. Ozaki, S. Delprat, M. Chaker, N. Thiré, B. E. Schmidt, F. Légaré, D. D. Klug, A. Y. Naumov, D. M. Villeneuve, A. Staudte, and P. B. Corkum, "Strong-field optoelectronics in solids," Nat. Photonics **12**(8), 465–468 (2018).
11. G. M. Gale, G. Gallot, F. Hache, and R. Sander, "Generation of intense highly coherent femtosecond pulses in the mid infrared," Opt. Lett. **22**(16), 1253–1255 (1997).
12. B. Golubovic and M. K. Reed, "All-solid-state generation of 100-kHz tunable mid-infrared 50-fs pulses in type I and type II $AgGaS_2$," Opt. Lett. **23**(22), 1760–1762 (1998).
13. R. A. Kaindl, M. Wurm, K. Reimann, P. Hamm, A. M. Weiner, and M. Woerner, "Generation, shaping, and characterization of intense femtosecond pulses tunable from 3 to 20 µm," J. Opt. Soc. Am. B **17**(12), 2086–2094 (2000).
14. P. Hamm, R. A. Kaindl, and J. Stenger, "Noise suppression in femtosecond mid-infrared light sources," Opt. Lett. **25**(24), 1798–1800 (2000).
15. T. Morimoto, N. Sono, T. Miyamoto, N. Kida, and H. Okamoto, "Generation of a carrier-envelope-phase-stable femtosecond pulse at 10 µm by direct down-conversion from a Ti:sapphire laser pulse," Appl. Phys. Express **10**(12), 122701 (2017).
16. D. J. Wilson, A. M. Summers, S. Zigo, B. Davis, S. J. Robatjazi, J. A. Powell, D. Rolles, A. Rudenko, and C. A. Trallero-Herrero, "An intense, few-cycle source in the long-wave infrared," Sci. Rep. **9**(1), 6002 (2019).
17. Y. V. Aulin, A. Tuladhar, and E. Borguet, "Ultrabroadband mid-infrared noncollinear difference frequency generation in a silver thiogallate crystal," Opt. Lett. **43**(18), 4402–4405 (2018).
18. L. Schmüser, S. Roeters, H. Lutz, S. Woutersen, M. Bonn, and T. Weidner, "Determination of Absolute Orientation of Protein α-Helices at Interfaces Using Phase-Resolved Sum Frequency Generation Spectroscopy," J. Phys. Chem. Lett. **8**(13), 3101–3105 (2017).
19. K. Kaneshima, N. Ishii, K. Takeuchi, and J. Itatani, "Generation of carrier-envelope phase-stable mid-infrared pulses via dual-wavelength optical parametric amplification," Opt. Express **24**(8), 8660–8665 (2016).

Optics EXPRESS

20. K. Liu, H. Liang, L. Wang, S. Qu, T. Lang, H. Li, Q. J. Wang, and Y. Zhang, "Multimicrojoule GaSe-based midinfrared optical parametric amplifier with an ultrabroad idler spectrum covering 4.2–16 μm," Opt. Lett. **44**(4), 1003–1006 (2019).
21. A. Leblanc, G. Dalla-Barba, P. Lassonde, A. Laramée, B. E. Schmidt, E. Cormier, H. Ibrahim, and F. Légaré, "High-field mid-infrared pulses derived from frequency domain optical parametric amplification," Opt. Lett. **45**(8), 2267–2270 (2020).
22. L. von Grafenstein, M. Bock, D. Ueberschaer, K. Zawilski, P. Schunemann, U. Griebner, and T. Elsaesser, "5 μm few-cycle pulses with multi-gigawatt peak power at a 1 kHz repetition rate," Opt. Lett. **42**(19), 3796 (2017).
23. T. Kanai, P. Malevich, S. S. Kangaparambil, K. Ishida, M. Mizui, K. Yamanouchi, H. Hoogland, R. Holzwarth, A. Pugzlys, and A. Baltuska, "Parametric amplification of 100 fs mid-infrared pulses in $ZnGeP_2$ driven by a Ho:YAG chirped-pulse amplifier," Opt. Lett. **42**(4), 683–686 (2017).
24. U. Elu, T. Steinle, D. Sánchez, L. Maidment, K. Zawilski, P. Schunemann, U. D. Zeitner, C. Simon-Boisson, and J. Biegert, "Table-top high-energy 7 μm OPCPA and 260 mJ Ho:YLF pump laser," Opt. Lett. **44**(13), 3194–3197 (2019).
25. S. Cheng, G. Chatterjee, F. Tellkamp, T. Lang, A. Ruehl, I. Hartl, and R. J. Dwayne Miller, "Compact Ho:YLF-pumped $ZnGeP_2$ -based optical parametric amplifiers tunable in the molecular fingerprint regime," Opt. Lett. **45**(8), 2255–2258 (2020).
26. L. von Grafenstein, M. Bock, D. Ueberschaer, E. Escoto, A. Koç, K. Zawilski, P. Schunemann, U. Griebner, and T. Elsaesser, "Multi-millijoule, few-cycle 5 μm OPCPA at 1 kHz repetition rate," Opt. Lett. **45**(21), 5998 (2020).
27. C. Gaida, M. Gebhardt, T. Heuermann, F. Stutzki, C. Jauregui, J. Antonio-Lopez, A. Schülzgen, R. Amezcua-Correa, A. Tünnermann, I. Pupeza, and J. Limpert, "Watt-scale super-octave mid-infrared intrapulse difference frequency generation," Light: Sci. Appl. **7**(1), 94 (2018).
28. J. Zhang, K. Fai Mak, N. Nagl, M. Seidel, D. Bauer, D. Sutter, V. Pervak, F. Krausz, and O. Pronin, "Multi-mW, few-cycle mid-infrared continuum spanning from 500 to 2250 cm−1," Light: Sci. Appl. **7**(2), 17180 (2018).
29. S. Vasilyev, I. S. Moskalev, V. O. Smolski, J. M. Peppers, M. Mirov, A. V. Muraviev, K. Zawilski, P. G. Schunemann, S. B. Mirov, K. L. Vodopyanov, and V. P. Gapontsev, "Super-octave longwave mid-infrared coherent transients produced by optical rectification of few-cycle 2.5-μm pulses," Optica **6**(1), 111–114 (2019).
30. V. Kozich, A. Moguilevski, and K. Heyne, "High energy femtosecond OPA pumped by 1030 nm Yb:KGW laser," Opt. Commun. **285**(21-22), 4515–4518 (2012).
31. S. B. Penwell, L. Whaley-Mayda, and A. Tokmakoff, "Single-stage MHz mid-IR OPA using $LiGaS_2$ and a fiber laser pump source," Opt. Lett. **43**(6), 1363–1366 (2018).
32. A. V. Mitrofanov, A. A. Voronin, D. A. Sidorov-Biryukov, S. I. Mitryukovsky, A. B. Fedotov, E. E. Serebryannikov, D. V. Meshchankin, V. Shumakova, S. Ališauskas, A. Pugžlys, V. Y. Panchenko, A. Baltuška, and A. M. Zheltikov, "Subterawatt few-cycle mid-infrared pulses from a single filament," Optica **3**(3), 299–302 (2016).
33. U. Elu, M. Baudisch, H. Pires, F. Tani, M. H. Frosz, F. Köttig, A. Ermolov, P. St. J. Russell, and J. Biegert, "High average power and single-cycle pulses from a mid-IR optical parametric chirped pulse amplifier," Optica **4**(9), 1024 (2017).
34. H. Liang, P. Krogen, Z. Wang, H. Park, T. Kroh, K. Zawilski, P. Schunemann, J. Moses, L. F. Dimauro, F. X. Kärtner, and K. H. Hong, "High-energy mid-infrared sub-cycle pulse synthesis from a parametric amplifier," Nat. Commun. **8**(1), 1–9 (2017).
35. S. Qu, H. Liang, K. Liu, X. Zou, W. Li, Q. J. Wang, and Y. Zhang, "9 μm few-cycle optical parametric chirped-pulse amplifier based on $LiGaS_2$," Opt. Lett. **44**(10), 2422–2425 (2019).
36. S. Qu, G. Chaudhary Nagar, W. Li, K. Liu, X. Zou, S. Hon Luen, D. Dempsey, K.-H. Hong, Q. Jie Wang, Y. Zhang, B. Shim, and H. Liang, "Long-wavelength-infrared laser filamentation in solids in the near-single-cycle regime," Opt. Lett. **45**(8), 2175–2178 (2020).
37. K. Liu, H. Liang, S. Qu, W. Li, X. Zou, Y. Zhang, and Q. J. Wang, "High-energy mid-infrared intrapulse difference-frequency generation with 5.3% conversion efficiency driven at 3 μm," Opt. Express **27**(26), 37706–37713 (2019).
38. B. M. Luther, K. M. Tracy, M. Gerrity, S. Brown, and A. T. Krummel, "2D IR spectroscopy at 100 kHz utilizing a Mid-IR OPCPA laser source," Opt. Express **24**(4), 4117–4127 (2016).
39. M. Mero, Z. Heiner, V. Petrov, H. Rottke, F. Branchi, G. M. Thomas, and M. J. J. Vrakking, "43 W, 1.55 μm and 1.25 W, 3.1 μm dual-beam, sub-10 cycle, 100 kHz optical parametric chirped pulse amplifier," Opt. Lett. **43**(21), 5246 (2018).
40. N. Thiré, R. Maksimenka, B. Kiss, C. Ferchaud, G. Gitzinger, T. Pinoteau, H. Jousselin, S. Jarosch, P. Bizouard, V. Di Pietro, E. Cormier, K. Osvay, and N. Forget, "Highly stable, 15 W, few-cycle, 65 mrad CEP-noise mid-IR OPCPA for statistical physics," Opt. Express **26**(21), 26907–26915 (2018).
41. N. Thiré, R. Maksimenka, B. Kiss, C. Ferchaud, P. Bizouard, E. Cormier, K. Osvay, and N. Forget, "4-W, 100-kHz, few-cycle mid-infrared source with sub-100-mrad carrier-envelope phase noise," Opt. Express **25**(2), 1505–1514 (2017).
42. T. Kanai, Y. Lee, M. Seo, and D. E. Kim, "Supercontinuum-seeded, carrier-envelope phase-stable, 4.5-W, 3.8-μm, 6-cycle, KTA optical parametric amplifier driven by a 1.4-ps Yb:YAG thin-disk amplifier for nonperturbative spectroscopy in solids," J. Opt. Soc. Am. B **36**(9), 2407–2413 (2019).

Optics EXPRESS

43. M. Knorr, J. Raab, M. Tauer, P. Merkl, D. Peller, E. Wittmann, E. Riedle, C. Lange, and R. Huber, "Phase-locked multi-terahertz electric fields exceeding 13 MV/cm at a 190 kHz repetition rate," Opt. Lett. **42**(21), 4367–4370 (2017).
44. B.-H. Chen, E. Wittmann, Y. Morimoto, P. Baum, and E. Riedle, "Octave-spanning single-cycle middle-infrared generation through optical parametric amplification in $LiGaS_2$," Opt. Express **27**(15), 21306–21318 (2019).
45. Y. Kim, I. Seo, S. W. Martin, J. Baek, P. Shiv Halasyamani, N. Arumugam, and H. Steinfink, "Characterization of New Infrared Nonlinear Optical Material with High Laser Damage Threshold, $Li_2Ga_2GeS_6$," Chem. Mater. **20**(19), 6048–6052 (2008).
46. A. Yelisseyev, Z. S. Lin, M. Starikova, L. Isaenko, and S. Lobanov, "Optical transitions due to native defects in nonlinear optical crystals $LiGaS_2$," J. Appl. Phys. **111**(11), 113507 (2012).
47. Y. Ni, H. Wu, C. Huang, M. Mao, Z. Wang, and X. Cheng, "Growth and quality of gallium selenide (GaSe) crystals," J. Cryst. Growth **381**, 10–14 (2013).
48. O. Isaienko and E. Borguet, "Ultra-broadband sum-frequency spectrometer of aqueous interfaces based on a non-collinear optical parametric amplifier," Opt. Express **20**(1), 547–561 (2012).
49. S. Akturk, X. Gu, P. Bowlan, and R. Trebino, "Spatio-temporal couplings in ultrashort laser pulses," J. Opt. **12**(9), 093001 (2010).
50. T. W. Golbek, L. Schmüser, M. H. Rasmussen, T. B. Poulsen, and T. Weidner, "Lasalocid Acid Antibiotic at a Membrane Surface Probed by Sum Frequency Generation Spectroscopy," Langmuir **36**(12), 3184–3192 (2020).
51. J. Schaefer, E. H. G. Backus, and M. Bonn, "Evidence for auto-catalytic mineral dissolution from surface-specific vibrational spectroscopy," Nat. Commun. **9**(1), 3316 (2018).
52. S. Malyk, F. Y. Shalhout, L. E. O'Leary, N. S. Lewis, and A. V. Benderskii, "Vibrational sum frequency spectroscopic investigation of the azimuthal anisotropy and rotational dynamics of methyl-terminated silicon(111) surfaces," J. Phys. Chem. C **117**(2), 935–944 (2013).
53. A. Sell, A. Leitenstorfer, and R. Huber, "Phase-locked generation and field-resolved detection of widely tunable terahertz pulses with amplitudes exceeding 100 MV/cm," Opt. Lett. **33**(23), 2767–2769 (2008).
54. O. Schubert, M. Hohenleutner, F. Langer, B. Urbanek, C. Lange, U. Huttner, D. Golde, T. Meier, M. Kira, S. W. Koch, and R. Huber, "Sub-cycle control of terahertz high-harmonic generation by dynamical Bloch oscillations," Nat. Photonics **8**(2), 119–123 (2014).
55. D. Gerz, W. Schweinberger, T. P. Butler, T. Siefke, M. Heusinger, T. Amotchkina, V. Pervak, U. Zeitner, and I. Pupeza, "Mid-infrared long-pass filter for high-power applications based on grating diffraction," Opt. Lett. **44**(12), 3014–3017 (2019).
56. V. Jukna, J. Galinis, G. Tamosauskas, D. Majus, and A. Dubietis, "Infrared extension of femtosecond supercontinuum generated by filamentation in solid-state media," Appl. Phys. B **116**(2), 477–483 (2014).
57. A.-L. Calendron, H. Çankaya, G. Cirmi, and F. X. Kärtner, "White-light generation with sub-ps pulses," Opt. Express **23**(11), 13866–13879 (2015).
58. D. T. Reid, P. Loza-Alvarez, C. T. A. Brown, T. Beddard, and W. Sibbett, "Amplitude and phase measurement of mid-infrared femtosecond pulses by using cross-correlation frequency-resolved optical gating," Opt. Lett. **25**(19), 1478–1480 (2000).
59. G. Tamošauskas, G. Beresnevičius, D. Gadonas, and A. Dubietis, "Transmittance and phase matching of BBO crystal in the 3–5 μm range and its application for the characterization of mid-infrared laser pulses," Opt. Mater. Express **8**(6), 1410–1418 (2018).
60. M. Woerner, A. Seilmeier, and W. Kaiser, "Reshaping of infrared picosecond pulses after passage through atmospheric CO_2," Opt. Lett. **14**(12), 636–638 (1989).
61. Z. Heiner, V. Petrov, and M. Mero, "Efficient, sub-4-cycle, 1-μm-pumped optical parametric amplifier at 10 μm based on $BaGa_4S_7$," Opt. Lett. **45**(20), 5692–5695 (2020).
62. A. Kurus, A. Yelisseyev, S. Lobanov, P. Plyusnin, M. Molokeev, L. Solovyev, D. Samoshkin, S. Stankus, S. Melnikova, and L. Isaenko, "Thermophysical properties of lithium thiogallate that are important for optical applications," RSC Adv. **11**(62), 39177–39187 (2021).
63. M. Neuhaus, H. Fuest, M. Seeger, J. Schötz, M. Trubetskov, P. Russbueldt, H. D. Hoffmann, E. Riedle, Z. Major, V. Pervak, M. F. Kling, and P. Wnuk, "10 W CEP-stable few-cycle source at 2 μm with 100 kHz repetition rate," Opt. Express **26**(13), 16074 (2018).
64. J. Pupeikis, P.-A. Chevreuil, N. Bigler, L. Gallmann, C. R. Phillips, and U. Keller, "Water window soft x-ray source enabled by a 25 W few-cycle 22 μm OPCPA at 100 kHz," Optica **7**(2), 168 (2020).
65. T. Feng, A. Heilmann, M. Bock, L. Ehrentraut, T. Witting, H. Yu, H. Stiel, S. Eisebitt, and M. Schnürer, "27 W 2.1 μm OPCPA system for coherent soft X-ray generation operating at 10 kHz," Opt. Express **28**(6), 8724 (2020).
66. M. Gebhardt, C. Gaida, F. Stutzki, S. Hädrich, C. Jauregui, J. Limpert, and A. Tünnermann, "Impact of atmospheric molecular absorption on the temporal and spatial evolution of ultra-short optical pulses," Opt. Express **23**(11), 13776–13787 (2015).